ULPGC Universidad de Las Palmas de Gran Canaria | Facultad de Ciencias del Mar

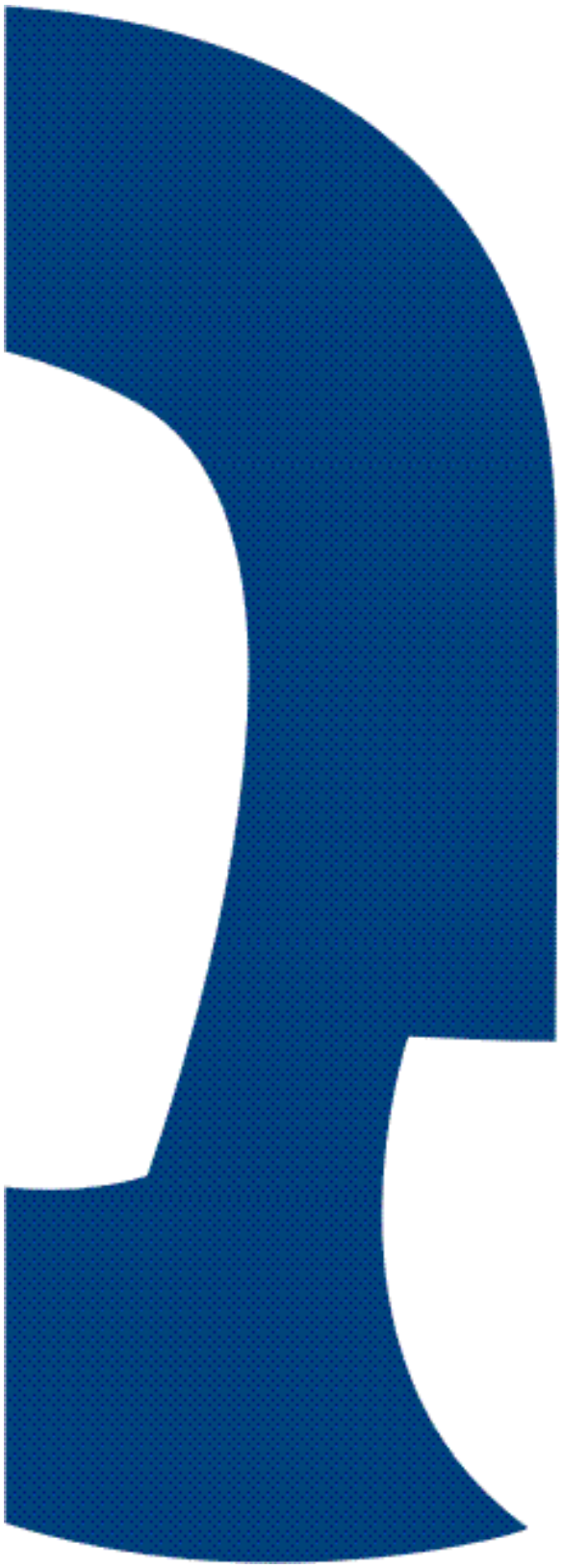

Lagrangian trajectories to assess marine plastic pollution distribution in the Canary Islands

Marcos Cividanes García

Curso 2021/2022

Tutores:

Francisco José Machín Jiménez

Miguel Borja Aguiar González

Trabajo Fin de Grado para la obtención del título de Graduado en Ciencias del Mar

Título:

Lagrangian trajectories to assess marine plastic pollution distribution in the Canary Islands.

Datos personales:

Nombre: Marcos

Apellidos: Cividanes García

Titulación: Ciencias del Mar

Datos del trabajo:

Tutor: Francisco José Machín Jiménez

Tutor: Miguel Borja Aguiar González

Empresa: Grupo de Oceanografía Física Y Geofísica Aplicada (OFYGA).

Departamento: Departamento de Física. Universidad de Las Palmas de Gran Canaria.

Firmas:

Estudiante: **Tutor**: **Tutor**:

Fecha: 01/07/2022

Contents

Acknowledgements:

I would like to thank the whole OFyGA group for accompanying me in the realization of this work, especially Borja Aguiar and Francisco José Machín for their motivation, patience, and perseverance, without whom this project would not have been possible.

I am also very grateful to Alicia Herrera, May Gomez and Ico Martínez, from the EOMAR group, for their willingness to collaborate with me in this and future studies.

Finally, I would also like to thank the indispensable support of my family and friends, who have never allowed me to give in to the stress of this work nor the rest of the degree.

Abstract: The increasing presence of plastics in the ocean is a harmful problem for marine ecosystems and the socio-economic sector. A recurrent type of debris gathered in waters of the Canary Islands are the identification tags employed at lobster traps deployed at the north-eastern coast of North America. Since 2016 to the present, these debris have been routinely collected and classified by the EOMAR group (MICROTROFIC Project) through coastal sampling focused on the eastern part of the Canary archipelago. In order to address this problem, a further understanding of the distribution and dynamics of these debris in the ocean is demanding. In this work, a pre-existing tool in Matlab has been upgraded to produce Lagrangian trajectories based on Marine Copernicus surface current velocity (GLORYS12V1). The main goal is to assess the trajectories that floating particles might follow in the North Atlantic subtropical gyre when released over a grid in the north-eastern coast of North America (Gulf of Maine). Our results provide a quantitative basis about the link between the North American north-eastern coast and the Canary Islands, where the presence of these and other debris is of increasing concern.

Key words: Plastic tags, Lagrangian trajectories, Distribution, Large-scale Circulation, North Atlantic Subtropical Gyre.

1. Introduction

It is well known that plastic waste has become one of the biggest environmental problems facing mankind. Their high demand, low cost and wide range of unique properties have made them essential for today's society (Scientific Advice Mechanism's (SAM) Goup of Chief Scientific Advisors, 2019). Therefore, the challenge of balancing the convenience that plastics bring to everyday life with their proper processing and recycling must be addressed (Galloway et al., 2017).

Despite this reality, between 4.8 and 12 million tonnes of plastic waste ends up in the ocean every year directly from coastal sources (Jambeck et al., 2015). Once there, these plastics break down over time into smaller pieces by mechanical abrasion and UV radiation (Van Sebille et al., 2020). This debris poses a major risk to marine ecosystems, as it can directly damage biota or even enter food chains, leading to cause problems of bioaccumulation and biomagnification due to the associated chemical additives (Miller et al., 2020).

In order to tackle this problem, a better understanding of the dynamic distribution of plastic debris in the ocean is demanding. However, the ocean exhibits an enormous variety of dynamic motions, ranging from millimetres to thousands of kilometres in scale. As seawater moves, each fluid particle carries tracers such as salt, nutrients and heat, as well as plankton and marine debris (Van Sebille et al., 2018).

In recent years, simulation tools for particle tracking in the oceans have undergone great improvements in terms of spatio-temporal resolution and computational optimisation, thus becoming a key complement to field and laboratory work (Hurlburt & Hogan, 2000; Werner et al., 2007).

From a Lagrangian approach we can use plastic debris as tracers to find out how water moves between ocean regions, the main pathways of movement, time scales, etc. This method is based on the use of virtual Lagrangian particles of zero special extension. For the determination of their trajectories, velocity fields are used, which can be given by OGCMs[1], observational measurements (such as surface geostrophic velocities based on satellite altimetry) or high-frequency radar measurements (Van Sebille et al., 2018).

On the occasion of the recurrent arrival of plastics tags in the Canary Islands, this work presents the results of the development of a Lagrangian particle tracking tool to provide a quantitative basis on the link between the arrival site of these plastics and the delivery site, the Gulf of Maine in the northeastern coast of the United States of America (USA).

1.1. Plastic tags from lobster traps

An exceptional case for implementing the traceability of plastics in the ocean is that of identification tags. They are present in everyday life in hundreds of activities, including fishing. Fishing involves licences, use of fishing gear, commercial and non-commercial purposes, and all of them must be specified. Thanks to these characteristics, once they are found, it is possible to estimate their place of origin or how long they have been in the water.

[1] Oceanic General Circulation Models.

Each year around 3 million traps are used for lobster fishing in the 7 lobster management areas (State of Maine - Department of Marine Resources, 2018). These areas are established in accordance with the USA government's management (Figure 1).

All these traps are identified by a code engraved on plastic tags that are attached to the device (State of Maine - Department of Marine Resources, 2022). From code, the following information can be obtained (from left to right): the license number of the fisherman (owner of the trap), the Lobster Management Area, the sequential tag number (ranging from 1 to 800 in most areas of the state), the state, the fishing season and finally the area within the state, (C. Fetterman[2] and K. Reardon[3], personal communication, June 15, 2022). An example of this code is shown in Figure 2.

Based on this information, the plastic tags from lobster traps become perfect tracers, as they allow us to identify both the geographical location of departure and estimate the time at which they might detach from the trap, then being at the mercy of the oceanic dynamics of the North Atlantic Ocean.

In addition to other debris, these plastic tags are being found on several beaches in the Canary Islands by the Marine Ecophysiology (EOMAR) group (Universidad de Las Palmas de Gran Canaria), which perform regular samplings every year since 2016.

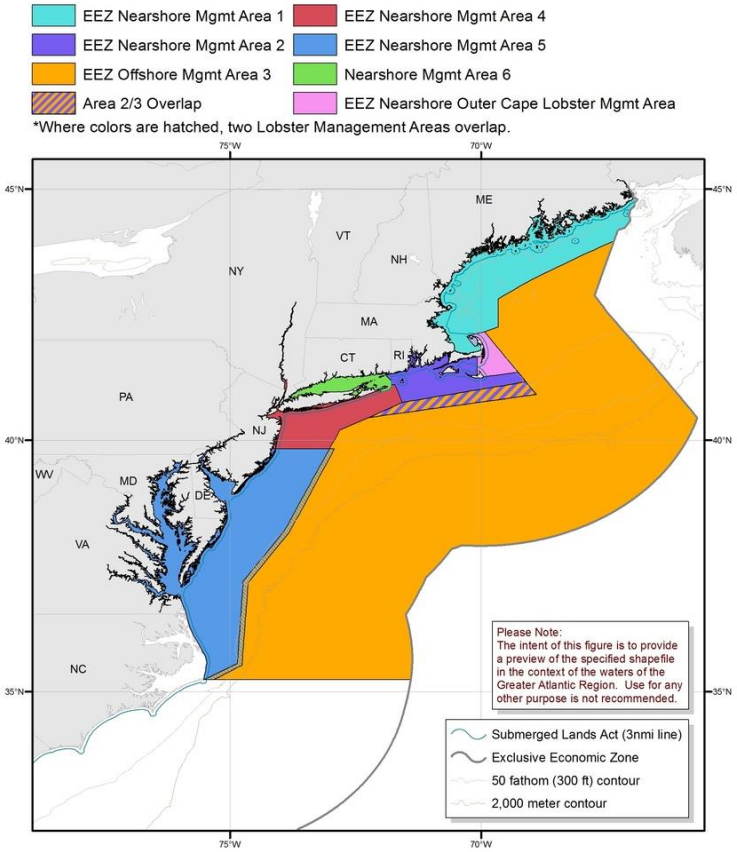

Figure 1. Map of lobster management areas. Source: Greater Atlantic Regional Fisheries Office.

[2] Director, Licensing Division. Dept. of Marine Resources. 21 State House Station. Augusta, ME 04333-0021

[3] Lead lobster fishery assessment biologist. Dept. of Marine Resources. 21 State House Station. Augusta, ME 04333-0021.

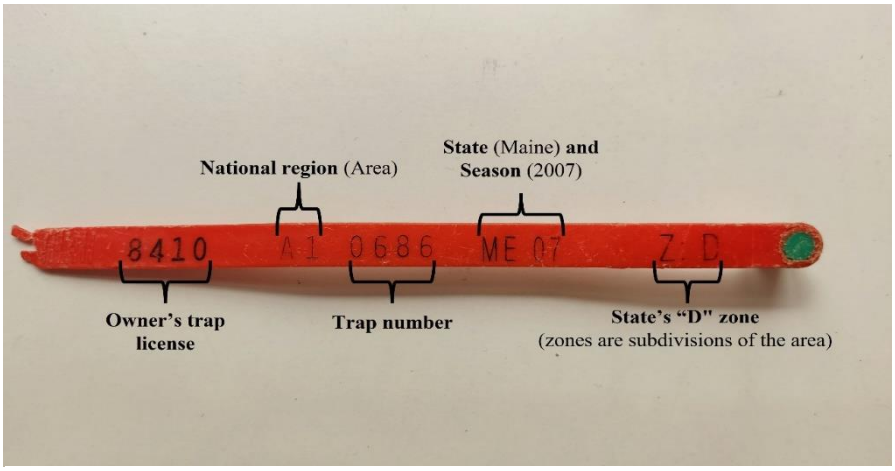

Figure 2. Example of a lobster trap tag code.

1.2. Study area and hypothesis

According to the finding of plastic tags from lobster traps deployed in the Gulf of Maine and arriving in the Canary Islands, three domains stand out as key for this study

- The lobsters fishing area in the Gulf of Maine USA. This is where lobster traps are deployed.

- The Canary Islands, Spain. This is where observational evidence supports the arrival of plastic tags from lobster traps originated in the Gulf of Maine.

- The North Atlantic Subtropical Gyre. This is the large-scale circulation feature embedding and connecting the two former areas.

1.2.1. Source area of the plastic tags: Gulf of Maine

The Gulf of Maine is a semi-enclosed coastal maritime enclave of the Northwest Atlantic shelf. The sea floor is bounded by three sedimentary structures: Georges Bank, Nantucket Shoals and Browns Bank. Also, it encloses three primary basins deeper than 200 meters (Lynch et al., 1996).

The Gulf of Maine is connected to adjacent waters by three main channels: the Grand South Channel between Nantucket Shoals and Georges Bank; the Northeast Channel between Georges Bank and Browns Bank, and the North Channel north of Browns Bank. In addition to these connections to adjacent waters, there are freshwater inflows from rivers and surface runoff from Maine and Nova Scotia (Lynch et al., 1996).

A circulation sketch of the Gulf of Maine is presented in Figure 3. This sketch is based on various observational, theoretical and modelling studies. The Gulf of Maine has two main inflows: on the one hand, through the North Channel (Nova Scotia shelf water); and, on the other hand, through the Northeast Channel (slope water). In contrast, the main outflow from the gulf occurs through the Great South Channel. In this region, prevailing closed circulation cells increase the residence times and retention capacity of the Gulf circulations (Lynch et al., 1996).

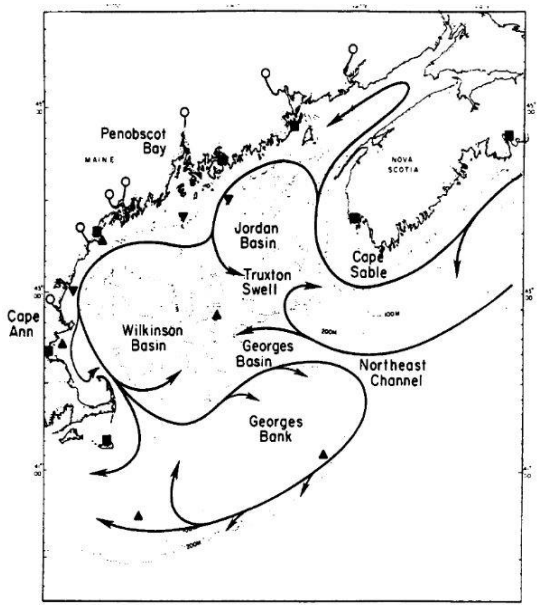

Figure 3. Schematic circulation in the Gulf of Maine (Lynch et al., 1996).

1.2.2. North Atlantic Subtropical Gyre

The North Atlantic Subtropical Gyre (NASG) is a wind-driven, clockwise gyre with large poleward transports in the western basin (Worthington, 1976), and smaller equatorward transports in the eastern basin (Stramma, 1984). The western part of the gyre is clearly dominated by the Gulf Stream (GS), which has very clear and intense signals, while the eastern part is dominated by weak currents with lower intensity signals (Stramma, 1984). Two zonal currents are also present, the Azores Current (AC) in the northeastern part of the gyre and the North Equatorial Current (NEC) in the southern part (Stramma & Müller, 1989).

The GS flows from the Gulf of Mexico northeastward along the North American coast, transporting approximately 30 Sv (Tychensky et al., 1998). Near Grand Banks (southeast of Newfoundland, Canada) the GS splits into two main branches; one of them flows northward to Europe, forming the North Atlantic Current (NAC), 20-25 Sv, and the other, 10-12 Sv, forms the AC, which flows eastward (Krauss, 1986; Sala et al., 2016; Tychensky et al., 1998).

The AC, the northernmost current of the NASG, has large meanders and loops, including mesoscale eddies with typical scales of 100-150 km (G. Siedler et al., 1985) which contributes to enormous variability (Tychensky et al., 1998). This current also splits into several branches (Fraile-Nuez et al., 2010), one of which penetrates the Gulf of Cadiz (Sala et al., 2016), while the easternmost branch feeds the Canary Current (CC) (Machín et al., 2006). This current, of lower intensity, flows southward along the African coast until it turns westward at approximately 20-25º N where it joins the NEC (Hernández-Guerra et al., 2005). The surface waters of these currents do not move south of the Cape Verde frontal zone (Michael D. Cox & Kirk Bryan, 1984), but flow westward (Tychensky et al., 1998) towards the Gulf of Mexico to close the gyre recirculation.

It is also worthwhile mentioning the inflow of Arctic Ocean waters that are exported to the North Atlantic via the Labrador Current (LC) (Sicre et al., 2014). Northwest of Newfoundland (Canada) the LC splits into two unequal branches, a larger one that is

trapped along the continental slope and a smaller one that flows over the Newfoundland shelf to the southwest (Lazier J. R. N. & Wright D. G., 1993). This subarctic water inflow is associated with the GS north of Cape Hatteras (Bersch, 2002).

The circulation of the NASG is represented schematically in Figure 4.

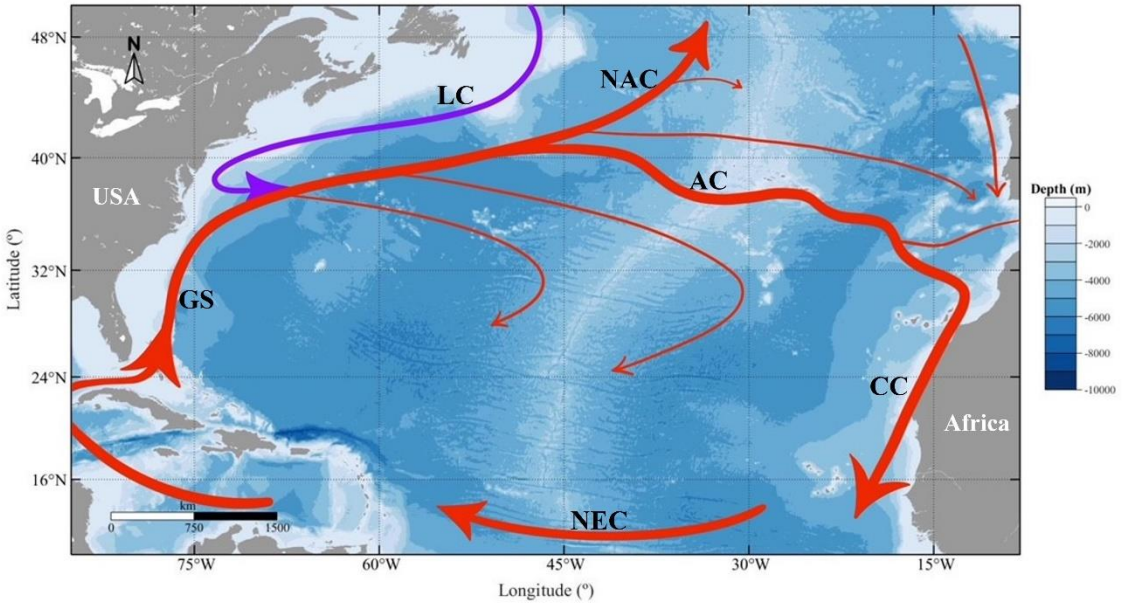

Figure 4. Bathymetric map of the North Atlantic Ocean. The arrows represent the surface currents of the North Atlantic Subtropical Gyre. The acronyms stand for: Labrador Current (LC), Gulf Stream (GS), North Atlantic Current (NAC), Azores Current (AC), Canary Current (CC) and North Equatorial Current (NEC).

1.2.3. Arrival area of the plastic tags: the Canary Islands

The Canary Islands are located at the eastern boundary of the North Atlantic basin between, roughly, 27º-29º N and 13º-18ºW. In this region, the archipelago is influenced by the two components of the Canary Current System (CCS): the CC, the eastern boundary current of the (NASG), and the Canary Upwelling Current (CUC) (Mason et al., 2011). The CC is a weak flow current that transports approximately 3 Sv in a southwesterly direction, parallel to the African coast, and occupies much of the central water layer (~ 0-700 m) (Fraile-Nuez & Hernández-Guerra, 2006; Machín et al., 2006). The origin of this current lies between Madeira and the African coast and is considered a natural extension of the AC as it approaches its easternmost boundary (Machín et al., 2006; Stramma, 1984). The CC is also fed by the Portugal Current, which flows southward off the Iberian Peninsula, although this is only clear during summer and autumn (Machín et al., 2006). The CC shows seasonal variability, such that it weakens and approaches Madeira towards winter, strengthening and centring between Madeira and the African coast towards summer (Stramma & Siedler, 1988). After passing through the Canary Islands, the CC joins the NEC north of Cape Verde (Hernández-Guerra et al., 2005).

The main surface circulation of the eastern NASG is schematically shown in Figure 5.

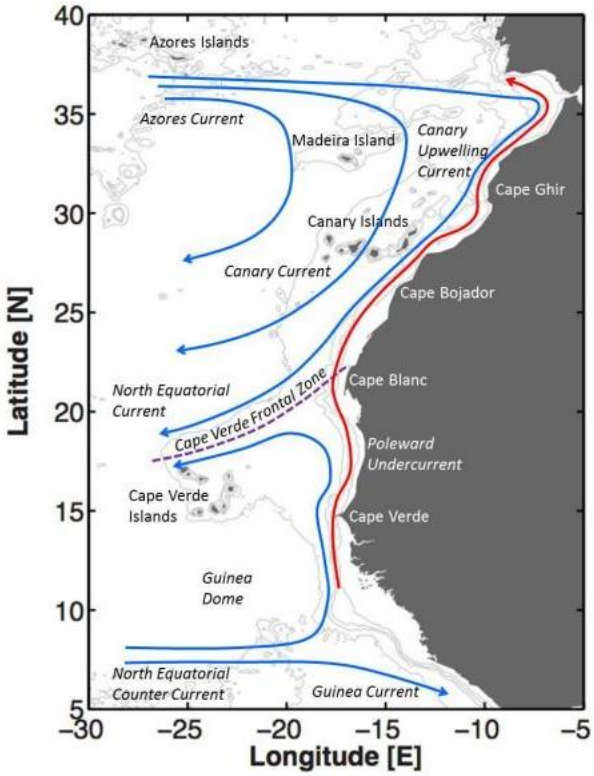

Figure 5. Schematic illustration of the main surface currents of the eastern NASG. The red arrow indicates the path of the Poleward Undercurrent (Josep L. PELEGRÍ & Jesús PEÑA-IZQUIERDO, 2015).

Given the above context in terms of large circulation patterns, it seems reasonable to expect that, the Canary Islands Archipelago will be recurrently receiving a large amount of plastic waste brought by currents, making it indeed a hot spot for the accumulation of marine litter that tends to be deposited on the north-eastern coast of the islands (Baztan et al., 2014; Herrera et al., 2018, 2022; Reinold et al., 2020).

Among all this waste, the lobster trap tags, documented for the first time in the Canary Islands on the Islet of Alegranza (Herrera et al., 2022), represent the best candidate to reconstruct the story of how upstream currents transport litter of different origin towards our area of study.

2. Data and methods

2.1. Sampling process

The collection and classification of plastic tags from lobster traps arriving in the Canary Islands have been carried out through coastal sampling by the EOMAR group under the umbrella of the MICROTROFIC Project. The first of these samplings was carried out in La Graciosa in 2016, where the abundance of this debris was significant. Since then, plastic tags have continued to be collected on other coasts, such as Lanzarote, Fuerteventura and Gran Canaria. In Figure 6, a graphical summary of plastic tags collected by years and islands is presented.

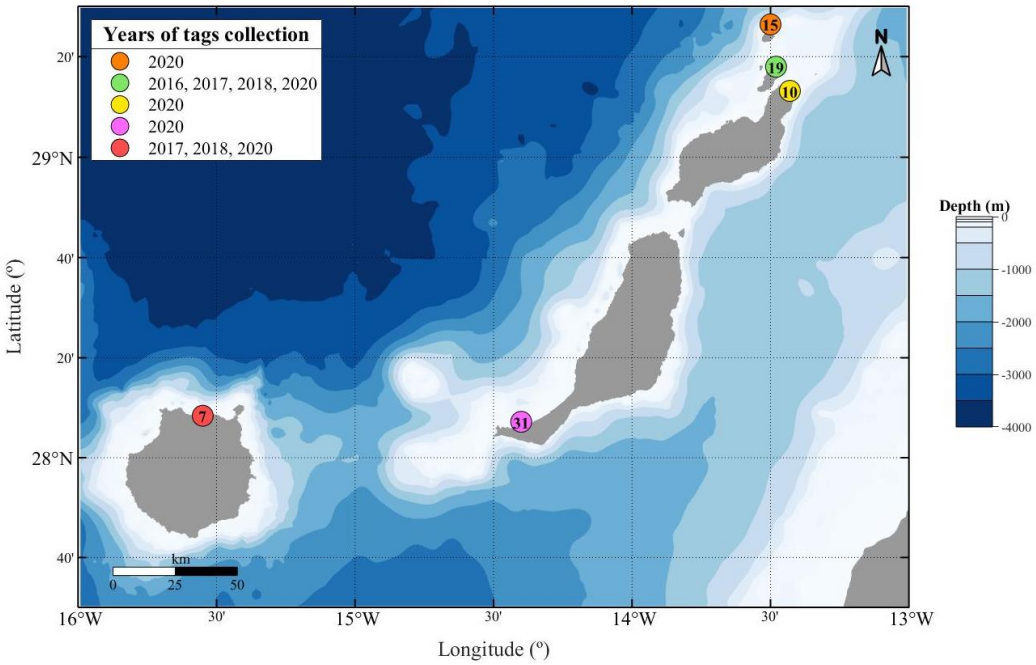

Figure 6. Bathymetric map of the eastern islands of the Canary Archipelago. The big dots represent the sampling areas where the tags were found by EOMAR group. The number inside of them is the total number of tags found in every area, and in the legend the reader will find in which years this number of tags has been collected.

In view of the continuous appearance of this type of recognizable waste, a call to citizen science participation was addressed, asking occasional beach and coastal users to report sightings of these plastic tags by means of photographs, descriptions and their location. The total number of tags collected up to October 2020 is shown in Figure 7.

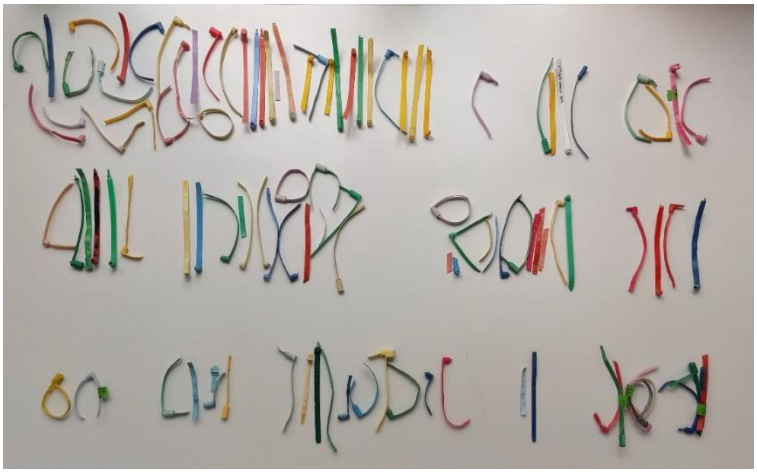

Figure 7. Plastic tags collected by EOMAR group between 2016 and 2020.

2.2. Particle releasing grid

In the north-eastern coast of the USA, there are seven Lobster Management Areas (Figure 1), labelled as follows: Area 1, 2, 3, 4, 5, 6, and the Outer Cape. Additionally, two stock areas are also defined: Gulf of Maine/Georges Bank (GOM/GBK) and Southern New England (SNE) (Greater Atlantic Regional Fisheries Office, 2020).

A large part of the plastic tags that arrived in the Canary Islands are of unknown origin regarding the Lobster Management Area they belonged to. However, more than half of the plastic tags the EOMAR group has collected in the Canary Islands originated from the Area1 (A1) (31 plastic tags out of a total of 41 plastic tags with readable code) (EOMAR group). Based on this finding, the present study focuses on a series of simulations where virtual particles are released at the Gulf of Maine (Figure 8). The particle release occurs along ten zonal transects extending from the coast to the outer shelf, and from 41.25ºN to 43.5ºN. The distance between consecutive zonal transects is 27.75 km. Within each transect, the distance between particles before being released is 5.55 km.

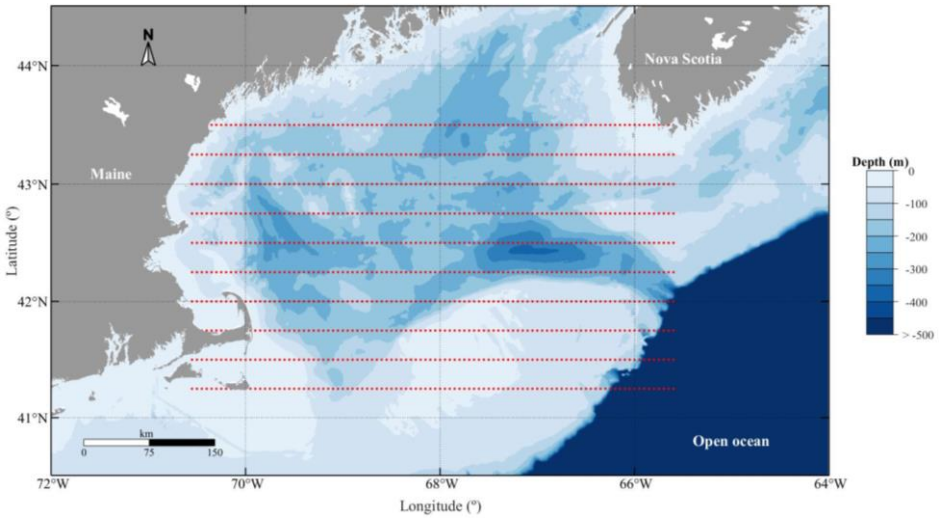

Figure 8. Bathymetric map of the Gulf of Maine. The red dots indicate the initial position of the virtual particle grid.

2.3. NAO index

In order to consider the effect of the North Atlantic Oscillation (NAO) on ocean circulation patterns, the NAO index was used for this study to choose a time interval for the study. This index varies from month to month according to the phenomenon. The data for this climatic index were obtained from the NOAA Climate Prediction Center (NOAA - Climate Prediction Center, 2022).

2.4. Particle tracking algorithm

A tool for Lagrangian tracking of passive particles of zero spatial extent has been developed by adapting a pre-existing tool, in principle working only on data extracted from HOPS (Harvard Ocean Prediction System) (Andrew Poje, 2008). The oceanographic scenario where the present study takes place requires a larger domain than the one offered by HOPS (regional modelling) and so the use of global ocean model is mandatory. This led to update the algorithm, to make it flexible enough to work efficiently (computational time) with input data from any model/observational format.

In this work, the particle tracking algorithm uses as input data the velocity fields from the GLORYS12V1 product, the CMEMS global ocean eddy resolution reanalysis. This product has a horizontal resolution of 1/12° (approximately 8km). Although 50 vertical levels are available, only surface data were used. The core component is the NEMO platform, forced at the surface by the ECMWF ERA-Interim and ERA5 reanalyses (Drévillon et al., 2021).

The Runge-Kutta numerical method was used to calculate the trajectories of each particle after their release at given location embedded in the modelled velocity field (see the grid for particle release in Figure 8). This method allows to solve differential equations with initial conditions when conventional methods (separation of variables) cannot be used.

Mathematically, this method works as follows:

$$\frac{dy(t)}{dt} = f(t,y)\,; \quad y(t_0) = y_0 \qquad (1)$$

where y is the equation to be solved, t is the time, y_0 is the value of the function at the initial instant, and t_0 is the value of the time at the initial instant. This is a high-precision one-step method called the fourth-order Runge-Kutta method as it usually takes four points in advance.

For the implementation of this method in Matlab, there is an internal program function called "ode45". This function works with the following syntax:

$$[t,y] = ode45(odefun, tspan, y_0) \qquad (2)$$

where $odefun$ is the differential equation we want to solve, $tspan$ is the time interval in which we want to solve the equation (and at the same time it sets the step size of the method), and y_0 is the initial condition of the equation.

With this mechanism, the system of equations was defined in order to apply the $ode45$ function. This was composed of the estimated particle velocities for each instant of time, for which it was necessary to interpolate the spatial variables (latitude and longitude taken to x-y space), time, the orthogonal components of the current velocity (U and V) and the estimated position of the particle at each instant. The method chosen for this interpolation was linear, due to its accuracy and the high computational cost of using other methods at the scale of work employed.

2.4.1. Algorithm optimization

The optimization of the algorithm was addressed in order to balance the computational time required for a given simulation to run with a large enough amount of particles being released.

The optimization was assessed following a series of tests with the aim of reducing the computational cost as much as possible so that we could extend the spatio-temporal scales of the Lagrangian simulations. The step of the algorithm that consumed most of the computational time was the interpolation of the variables. To optimize this step, we avoided bringing the entire time domain of the velocity field into Matlab workspace.

Instead, by means of a loop, only the fields corresponding to the two consecutive times necessary for the calculation of the trajectory were loaded. This modification allowed simulations of longer duration to be carried out.

Lastly, different tests were also performed with different numbers of particles in relatively short simulations. It was observed that increasing the number of particles progressively from 10 to 1000 had no effect on the computational time needed to calculate the trajectories, so a grid of 1000 particles was established for the successive experiments. Since this is a quantity that allows a large amount of information to be extracted, and in order not to increase the computational cost of the subsequent representations of the trajectories, it was decided not to increase the density of particles in the grid even further.

3. Results

3.1. *Time travel of plastic tags*

As a first approach in the study of the oceanic circulation of plastic tags of lobster traps, the time elapsed between their season of use and the time of collection by EOMAR group at the sampling points (Figure 6) was analyzed. The results are shown in Figure 9.

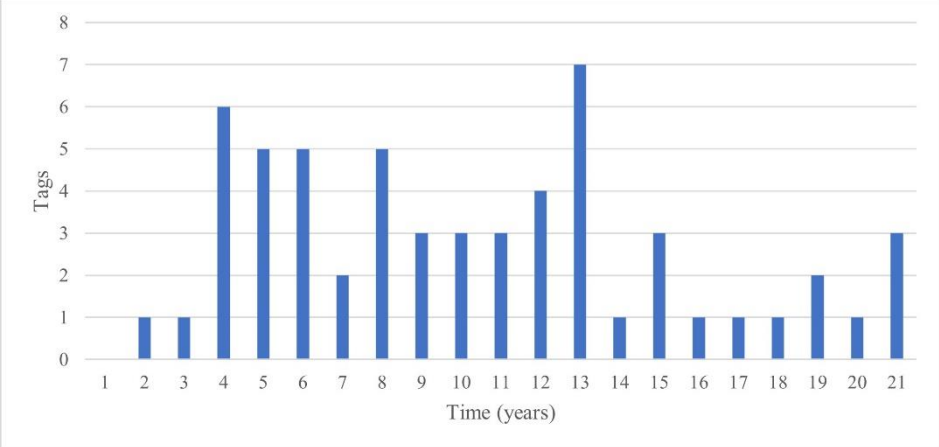

Figure 9. Time elapsed from the use of the tags to their collection by EOMAR group. Only tags with readable code are recorded.

Due to the irregularity of sampling at some of the beaches, it was not considered appropriate to talk about maximum or average times of travel. On the other hand, the minimum travel times were considered relevant, since they provide a first idea of the minimum time it may take for these tags to reach the Canary Islands.

As it can be seen in Figure 9, a tag arrived in only 2 years, so after studying the seasonal variability, we worked with a simulation of this duration in order to find out if the particles arrive in the vicinity of the Canary Islands after that time.

3.2. Choice of time interval for experimentation

There is evidence that the position of the GS is influenced by the North Atlantic Oscillation (NAO) with a certain delay (Watelet et al., 2017). Since it is the NASG stream that first affects the particle release area (Figure 8), and with the goal of reducing as much as possible the variables affecting particle dispersion, it has been estimated which year has an average NAO index closest to 0.

For this purpose, a graphical representation of the monthly NAO index (Figure 10) and a root mean square of the sum of these squared values (Table 1) has been made.

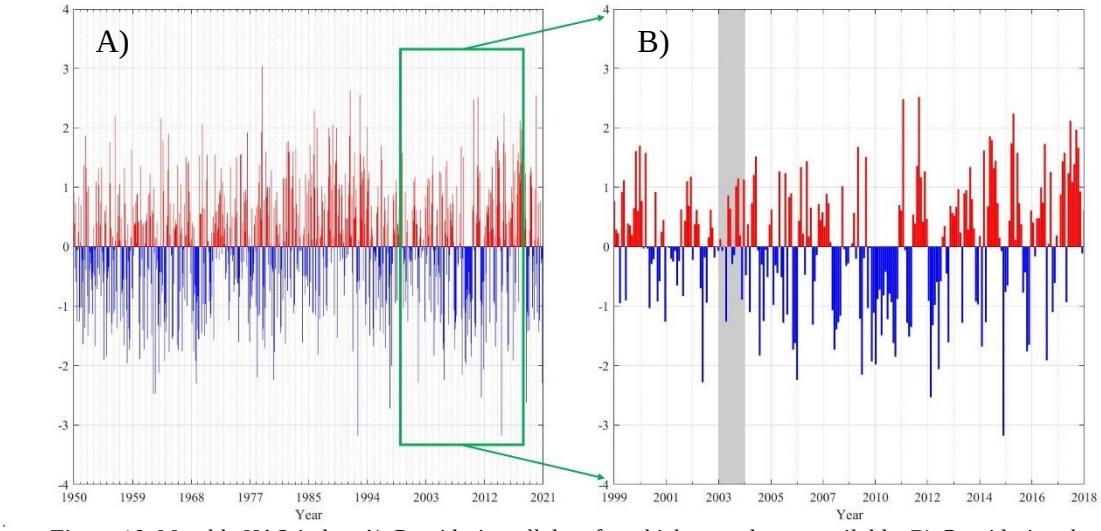

Figure 10. Monthly NAO index. A) Considering all data for which records are available. B) Considering the time interval based on the oldest and the newest plastic tag sampled (EOMAR group). Data Source: NOAA Climate Prediction Center (NOAA - Climate Prediction Center, 2022).

Year	Mean NAO index	Year	Mean NAO index
2003	0.5251	2008	0.9825
2001	0.5421	2017	1.0166
2007	0.7102	2014	1.1335
1999	0.8103	2009	1.1683
2004	0.8243	2012	1.2338
2013	0.8557	2010	1.2429
2005	0.8833	2006	1.3067
2000	0.8925	2011	1.3594
2016	0.9391	2018	1.3695
2002	0.9398	2015	1.4989

Table 1. Ordered results of root mean square of the sum of monthly NAO index squared values between 1999 and 2018.

Considering the results, 2003 was the year chosen for the following experimentation.

3.3. Two-year simulation

Starting on 1/1/2003, a two-year simulation was performed on an exploratory basis. To observe their geographic distribution of the particles, particle counting was performed in 1.25°*1.25° cells after 6, 12, 18 and 24 months of simulation, as shown in Figure 11.

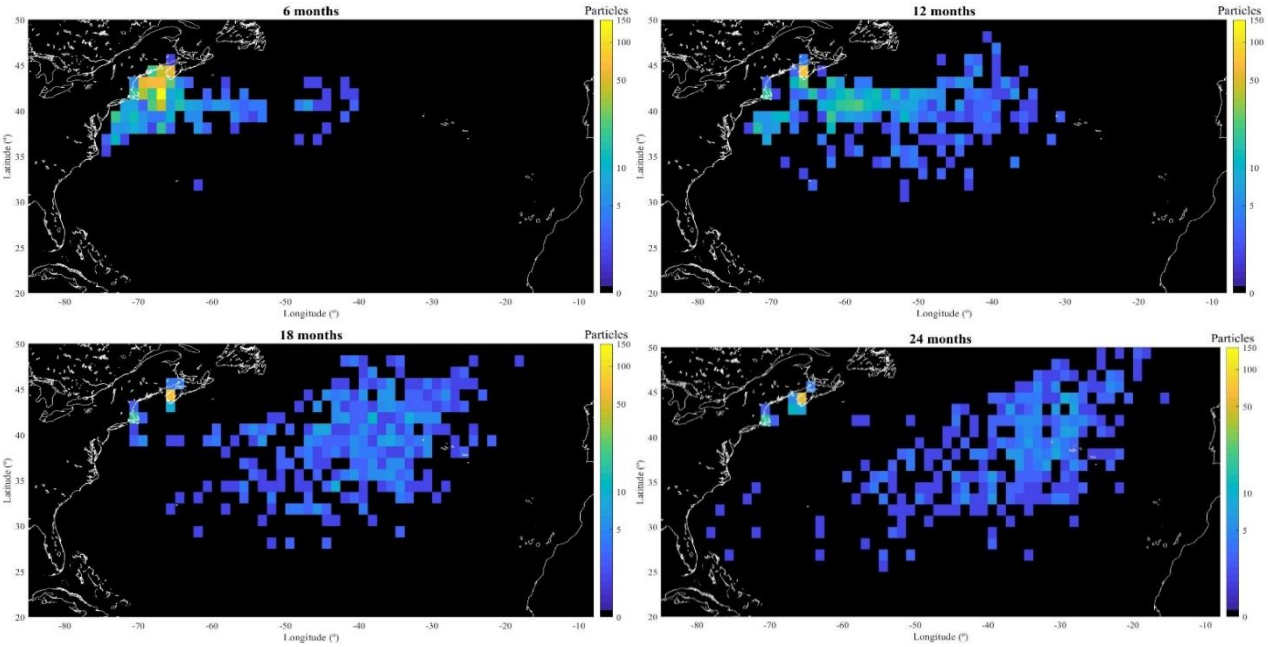

Figure 11. Particle density in the North Atlantic basin after 6, 12, 18 and 24 months of simulation.

To quantify this distribution at the end of the simulation (after 2 years), a more exhaustive analysis was performed. For this purpose, a particle count was again prepared in cells of larger size (2.5ºx2.5º) than the one used in Figure 11. The results are shown in Figure 12.

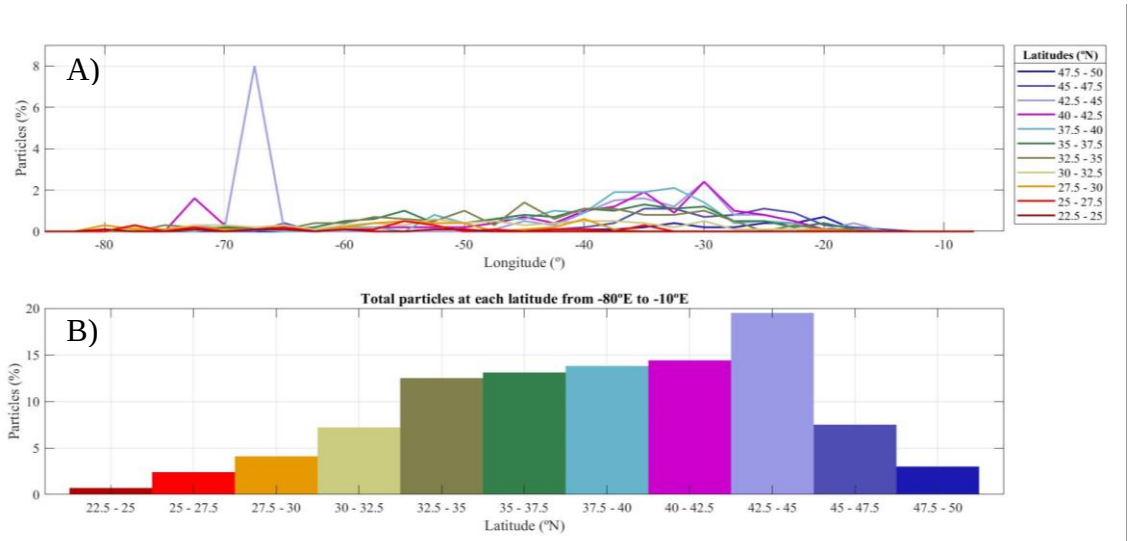

Figure 12. Geographical distribution of particles after simulation from 01/01/2003 to 12/30/2004. A) Percentage of particles with respect to longitude at different latitudes. B) Total percentage of particles from -80ºE to -10ºE at each 2.5º latitude interval.

In Figure 12(A) it can be seen how the 40-45ºN band presents a peak of particles between -75 and -65 ºE. This peak is especially intense between 42.5-45ºN, reaching

8% of the total particles. This geographical frame coincides with the proximity of the releasing zone (Figure 8). Except for this fact, it is observed how, with small ups and downs, the amount of particles increases in a generalized way as one moves eastward, presenting a second maximum (~2%) around -30ºE.
Figure 12(B) shows that the particles tend to be located in the northern part of the North Atlantic Subtropical Gyre (NASG), although some exceed these latitudes (45-50ºN).
Combining both views, it is extracted that, after two years of simulation, the particles tend to be located in the northeastern part of the NASG, although many particles do not follow this rule and are trapped in the launch zone or follow different trajectories.

3.4. Seasonal variability

As it can be seen, most of this dispersion is eastward, as expected according to NASG dynamics. With this observation, the motivation arises to study whether there is notable differences in the early stages (outflow from Gulf of Maine to NASG) of particle dispersion, starting at different times of the year. For this purpose, 12 simulations were carried out, with a duration of 90 days each, starting on the 1st day of each month of 2003.

Given the hypothesis that all the particles in the grid might not move in the same way, they were classified, according to their position of origin, into 4 quadrants of 250 particles (NW, NE, SW, SE).

In order to characterize the results obtained the effective distances, propagation speeds and deflection angles are estimated, which are presented below.

3.4.1. Effective Distance

Two procedures were followed to calculate the distance traveled by the particles:

- Considering the cumulative effective distance of each particle and average it among all particles in each quadrant, obtaining a daily result for each month and quadrant (Figure 13).
- Considering the straight-line distance in kilometers between the initial position and the final position for each particle in each quadrant, obtaining a single result for each particle, month and quadrant (Figure 14).

Figure 13 shows how there are seasonal differences in the effective distance traveled by particles in the four quadrants. Spring (green) and summer (red) months tend to be more clustered in all cases than autumn (mustard) and, especially, winter (blue) months, where greater differences are found. December is the month with the greatest effective distances, except in the NE quadrant, where it is exceeded by other months in the upper half. On the other hand, February has the lowest effective distances in all four cases, together with March.

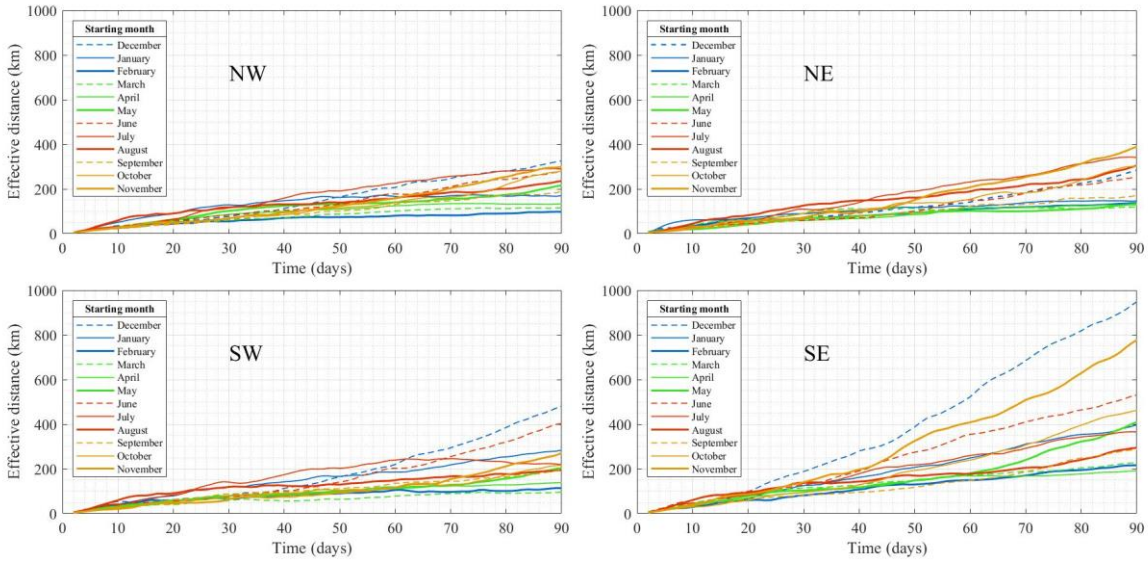

Figure 13. Cumulative effective distance (km) averaged over the 250 particles in each quadrant over time (days) for the different simulation months.

It can therefore be said that there is a certain pattern in which particles travel longer distances being released in December, and this decreases progressively until February, where low distance values stabilize also for the spring months. Subsequently there is a further increase towards June, which decreases again by August and finally increases towards November, which would link with December.

As for the differences between quadrants, the SE quadrant is noteworthy, with effective distances notably greater than the others in all months. This is followed by the SW quadrant and, below both, the NW and NE without notable differences.

Figure 14 corroborates the above. Starting in the spring months, most of the particles present low effective distances, with little difference between March, April and May. Beginning in the summer months, the histograms show lower peaks, indicating that the particles occupied a greater range of distances traveled and went farther than when launched in the spring. In the autumn months, a similar distribution is found as in the summer months. Finally, the winter months show the greatest variability between December, January and February. The latter presents in all quadrants very high particle peaks between 0 and 300 km. On the other hand, December shows very little particle clustering, with distances traveled from 0 to more than 2000 km, with a slight majority clustered around 500 km. In January, on the contrary, a high particle clustering is observed, but at higher distances than in February.

Differentiating between quadrants again shows that the particles in the SE quadrant have the longest distances traveled, with a large dispersion of particles over the entire range of distances. The rest of the quadrants do not present notable differences.

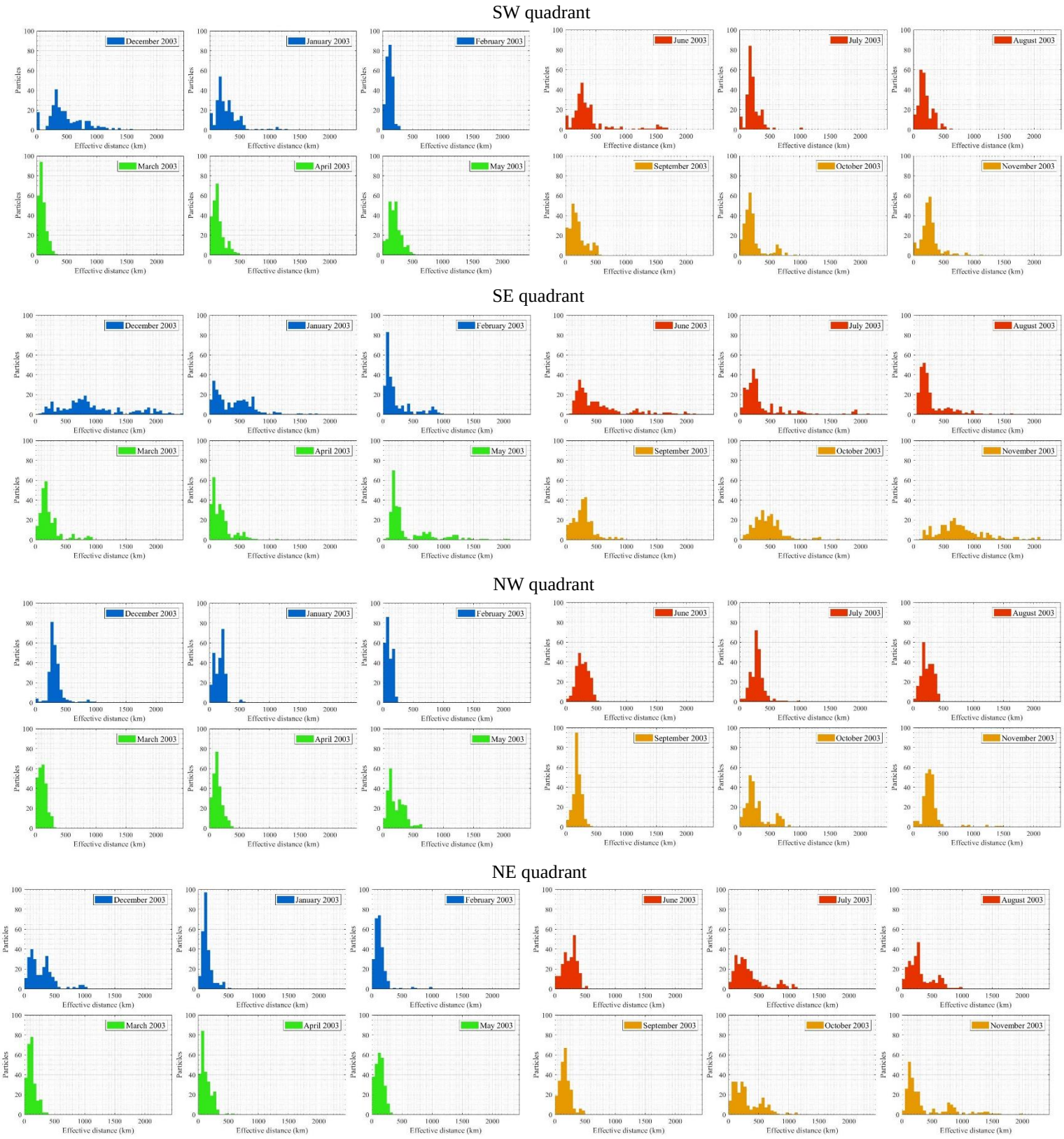

Figure 14. Distance in kilometers between the initial position and the final position for each particle of each quadrant on each starting month.

3.4.2. Propagation speed

For the calculation of the propagation velocity, two different procedures have also been followed:

- Considering the velocity in meters per second of each particle each day of the simulation and averaging it among all the particles in each quadrant, obtaining a daily result for each month and quadrant. Subsequently, a moving average with a step size of 7 days was applied to smooth the signal (Figure 15).
- Considering the propagation velocity in meters per second of each particle, averaged over the simulation, obtaining a result for each particle, month and quadrant (Figure 16).

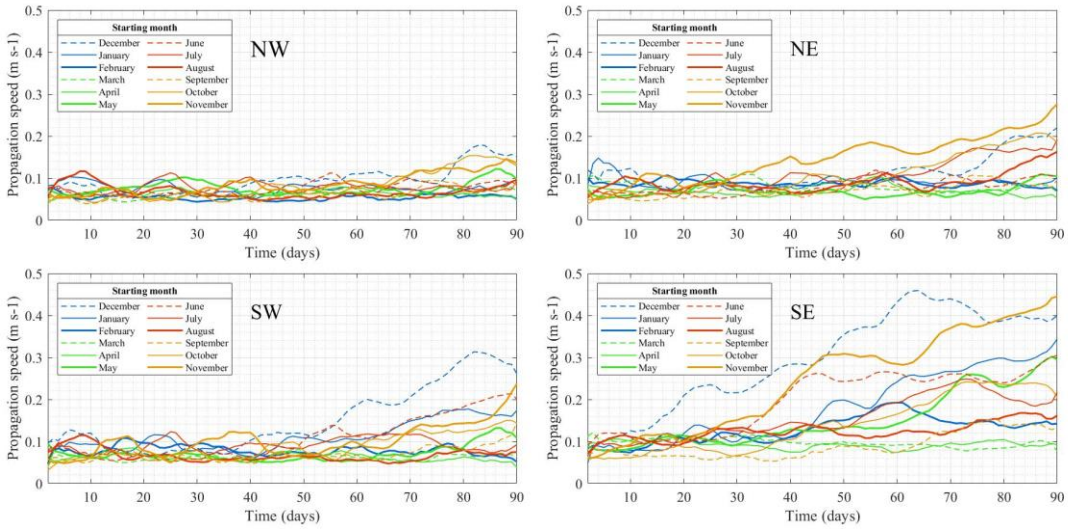

Figure 15. Propagation velocity (m s^{-1}) averaged over the 250 particles in each quadrant with respect to time (days) for the different simulation months.

As for the averaged propagation velocity (Figure 15), it can be observed how it varies according to the month and quadrant. Initially, all months are oscillating around 0.1 ms-1 until, after a certain instant, different in each quadrant and month, this velocity begins to increase. Except for the NE quadrant, the month that starts the acceleration earlier is December, which also has the highest velocities. This month is followed by November, which dominates the graph of the NE quadrant. The rest of the months are distributed similarly to what was observed in section 3.2.1., with few differences between the spring months and February, which are grouped together without varying much from their initial velocity. In addition, it can be generally observed that in the month of May the acceleration starts from day 80 of the simulation (day 50-55 in SE quadrant) while February and the other spring months do not show a significant increase in velocity throughout the simulation.

SW quadrant

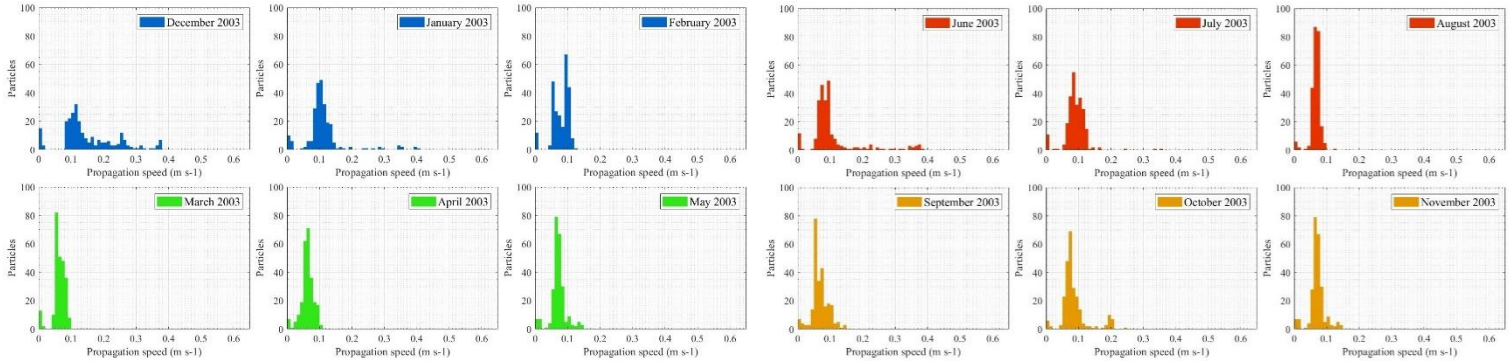

SE quadrant

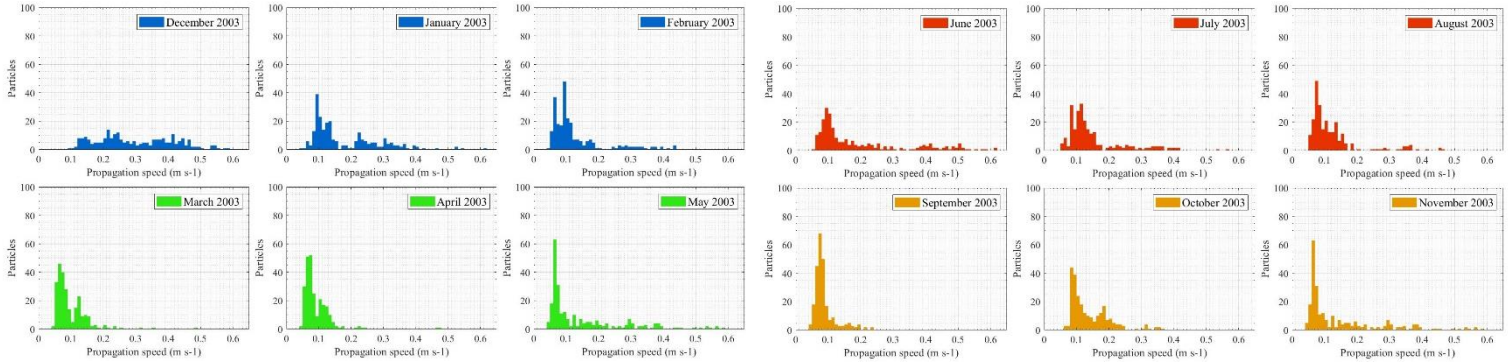

NW quadrant

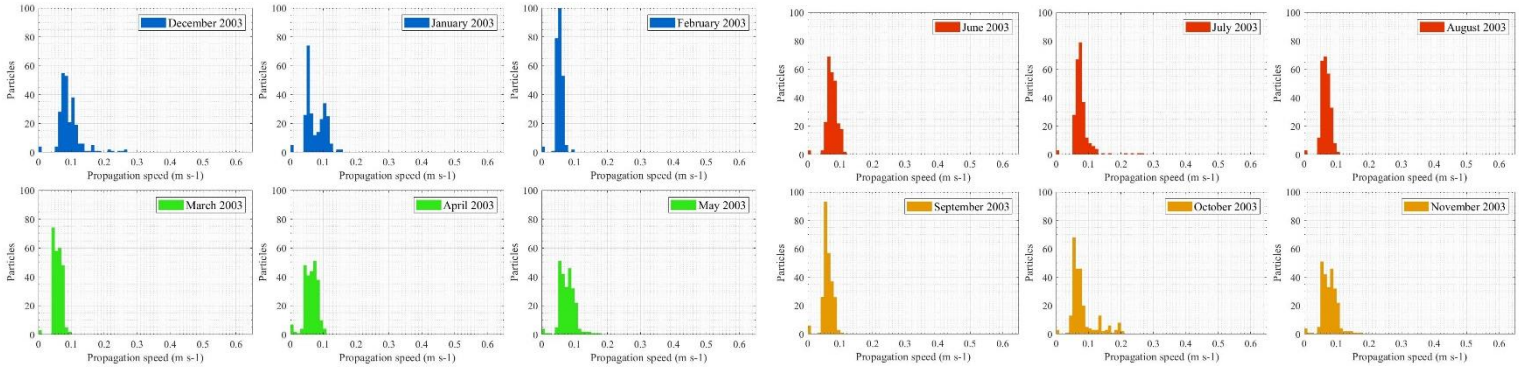

NE quadrant

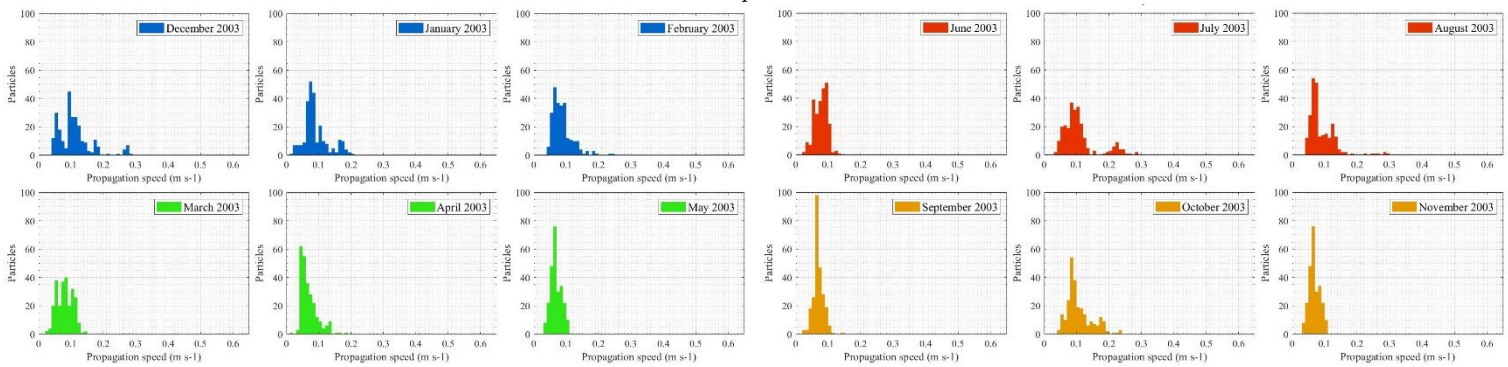

Figure 16. Velocity in meters per second of each particle averaged over the entire simulation for each quadrant and starting moth.

Looking at Figure 16 the same conclusions are obtained. The spring months and February present a large peak of particles around 0.1 m/s. This happens in some quadrants also for August/September. December, January and June instead present particles with very different average velocities, even exceeding 0.6 m/s (SE quadrant).
Once again, the SE quadrant shows greater variability among its particles and reaches higher velocity values, as in the previous section.
Analyzing especially the two quadrants of the southern half of the grid, an oscillatory seasonal pattern is suggested. That is, the particle velocity increases earlier and reaches higher values starting in December, which decreases progressively until March and April, increasing again towards June, which does not reach the same values as December, and it decreases again until September to finally increase towards November.

3.4.3. Deflection angle

For the calculation of the deflection angle, the angle formed by the straight line joining the initial and final position of each particle has been taken into account, considering E=0º, N=90º, W=180º, S=270º. For this calculation, the classification of the particles into quadrants was also considered, obtaining an angle for each particle, quadrant and starting month. With these results, a histogram in the form of a wind rose for each case, shown in Figure 17, was elaborated.

Analyzing Figure 17, it can be seen how some months present a predominant particle propagation direction (e.g., December and June SE quadrant) and a certain relationship according to seasonality. It can be said, in the same way as in section 3.2.1. and 3.2.2., that there is a certain seasonal pattern in which, starting in the winter months, the particles end up south-southeast of their initial position, which becomes east-southeast in the summer months. In the spring months there are no predominant directions, and in the autumn months there is a clear transition from September to November, so that in September the particles tend to end to the east of their initial position, in October to the east-southeast and in November to the south-southeast.

SW quadrant

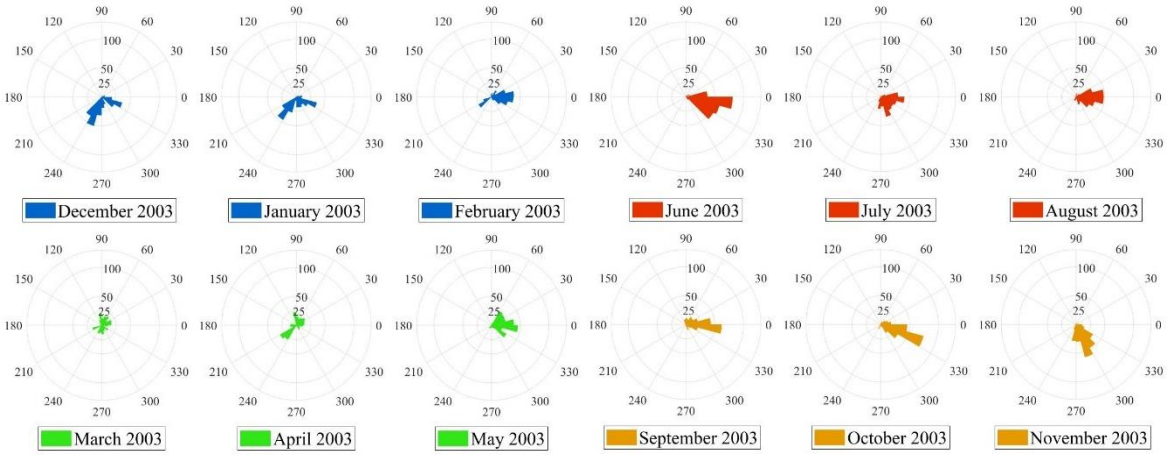

SE quadrant

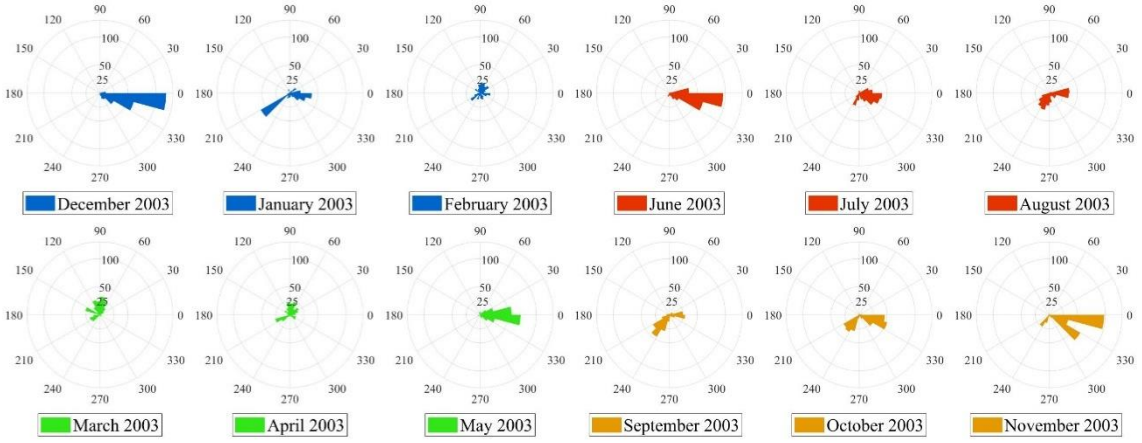

NW quadrant

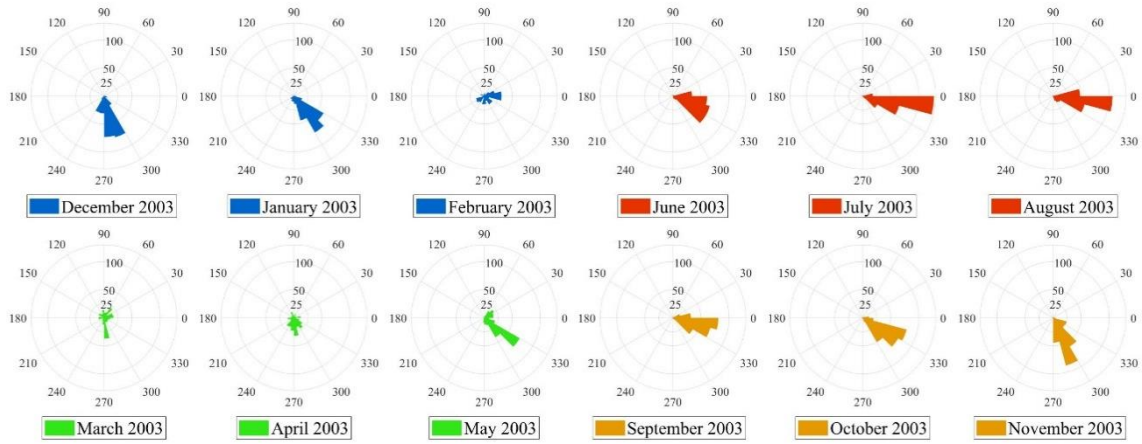

NE quadrant

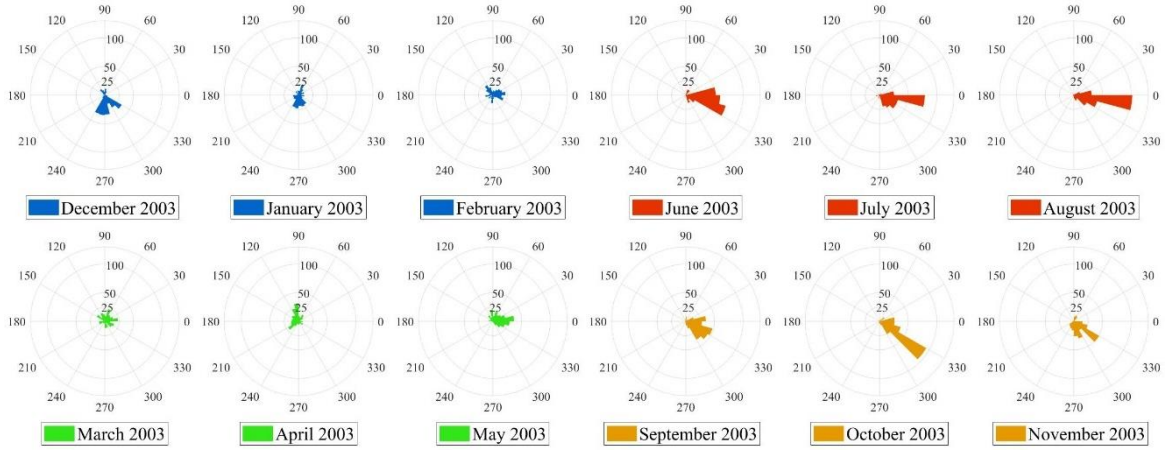

Figure 17. Deflection angle of each particle considering the initial and final position and differentiating between each quadrant and initial month.

4. Discussion

The increasing presence of plastics in the marine environment is an atrocity and an example of poor waste management in today's society. However, these plastics are unique tracers that provide an opportunity to expand our knowledge of the ocean's physical dynamics and transport pathways (Van Sebille et al., 2018).

The developed tool for Lagrangian tracking of particles in this study has proven to be operational and to show consistent results in terms of particle distribution and time scales (Wang et al., 2021; Werner et al., 2007). Its adaptation to work with data from different sources (OCM, altimetry, satellite) and its optimization to work with a large volume of particles in large areas make it a very useful factor for this and subsequent studies.

The particle tracking in this study has demonstrated connectivity between the northeast coast of the USA and the East of the North Atlantic Subtropical Gyre, where particles tend to terminate after two years of simulation. However, one must take into account a certain percentage of particles (~2.5% in this study) that exit to higher latitudes, probably driven by the GS branch that feeds the NAC to northern Europe (Krauss, 1986). From Figure 11 and Figure 12 it can also be deduced that the particles present a greater latitudinal dispersion as they leave the influence of the GS and enter the zone of the beginning of the NAC and the AC.

It has also been found that the initial phase (~3 months) of particle dispersion is influenced by the season of the year. Depending on the starting month, particles can travel more than twice the distance compared to other months (Figure 13 and Figure 14) and end up in very different directions compared to their initial position (Figure 17). In this way it can be determined in which months the particles are expected to go more directly eastward.

The differences between the SE quadrant and the other 3 quadrants in which the particle grid was subdivided have been attributed to the fact that this quadrant is less embedded in the Gulf of Maine, so that it can be less influenced by its retentive dynamics (Lynch et al., 1996) and enter the GS more quickly. This would explain that the acceleration in the propagation velocity increases in fewer days than in the other quadrants (Figure 15) and that the cumulative effective distances are greater (Figure 13), always considering that a common period of 90 days was used.

In contrast, the SW and the northern half quadrants are directly influenced by the retentive dynamics of the Gulf (circulation section) so that they take longer to exit into the NASG currents or even do not exit at all, being trapped towards the Bay of Fundy, which also explains the high percentage of particles (~8%) at 42.5-45N, -65ºE in Figure 12.

With these ideas it can be concluded that a plastic tag released in the least boxed point of the Gulf of Maine will have a more favorable trip to the Canary Islands, at least, considering its entry into the influence of the NASG. The same applies to the release of plastic tags in the months of June, November or December.

The main source of propulsion of plastic tags across the gyre and northward is the GS, suggesting that there is also a clear influence by the NAO, which the position of the

current depends on. Previous works (Bersch, 2002; de Coëtlogon et al., 2006; Taylor & Stephens, 1998) express the lag between changes in the NAO and the response of the GS as ~2 years, while other works express that the response occurs in a variable interval, between 0 and 2 years approximately (Watelet et al., 2017). For this reason, it would be of interest to repeat this study considering two years after the year chosen here, i.e., 2005, as well as to study the influence of positive and negative NAO situations on particle dispersion.

Finally, no particles from the long simulation reached the Canary Islands. This fact may be due to several factors:

- Stokes drift has not been considered.
- That the year and month of departure chosen were not optimal for the arrival of particles in only two years.
- That the arrival of tags in a time of two years was a coincidence, remembering that only one of the tags arrived in that time (Figure 9).

5. Conclusions

Some conclusions can be drawn from the results presented in this study:

- The developed tool for Lagrangian particle tracking shows results consistent with reality.
- The northeastern United States is connected to the eastern margin of the North Atlantic Basin through the NASG.
- Considering that the tags follow the results obtained in the simulations, those that escape the retentive dynamics of the Gulf of Maine are likely to be captured by the Gulf Stream.
- Particles show acceleration and travel longer distances since they enter the influence of the Gulf Stream.
- Deflection angles show that particles tend to end up east and southeast of their initial position after 90 days of simulation.
- February, March, April, and May appear to be the months in which the outflow of particles from the Gulf of Maine to the NASG is less favorable. In contrast June, November, and December are the months when this outflow appears to be much more rapid.
- Particles appear to show greater latitudinal dispersion and lower propagation velocities as they leave the influence of the Gulf Stream and enter the onset of the Azores and North Atlantic currents.
- It would be of interest for future studies to repeat the work for other years, considering longer time periods and different situations of the North Atlantic Oscillation, as well as to increase the number of particles released in each simulation.

6. Bibliography

Andrew Poje. (2008, September). *Matlab Scripts for constructing Lagrangian Trajectories in HOPS*. https://www.math.csi.cuny.edu/~poje/HOPS/

Baztan, J., Carrasco, A., Chouinard, O., Cleaud, M., Gabaldon, J. E., Huck, T., Jaffrès, L., Jorgensen, B., Miguelez, A., Paillard, C., & Vanderlinden, J. P. (2014). Protected areas in the Atlantic facing the hazards of micro-plastic pollution: First diagnosis of three islands in the Canary Current. *Marine Pollution Bulletin*, *80*(1–2), 302–311. https://doi.org/10.1016/J.MARPOLBUL.2013.12.052

Bersch, M. (2002). North Atlantic Oscillation–induced changes of the upper layer circulation in the northern North Atlantic Ocean. *Journal of Geophysical Research*, *107*(C10). https://doi.org/10.1029/2001JC000901

de Coëtlogon, G., Frankignoul, C., Bentsen, M., Delon, C., Haak, H., Masina, S., & Pardaens, A. (2006). Gulf Stream Variability in Five Oceanic General Circulation Models. *Journal of Physical Oceanography*, *36*(11), 2119–2135. https://doi.org/10.1175/JPO2963.1

Drévillon, M., Fernandez, E., & Lellouche, J. M. (2021). *PRODUCT USER MANUAL For the Global Ocean Physical Multi Year product GLOBAL_MULTIYEAR_PHY_001_030*. https://doi.org/https://doi.org/10.48670/moi-00021

Fraile-Nuez, E., & Hernández-Guerra, A. (2006). Wind-driven circulation for the eastern North Atlantic Subtropical Gyre from Argo data. *Geophysical Research Letters*, *33*(3). https://doi.org/10.1029/2005GL025122

Fraile-Nuez, E., Machín, F., Vélez-Belchí, P., López-Laatzen, F., Borges, R., Benítez-Barrios, V., & Hernández-Guerra, A. (2010). Nine years of mass transport data in the eastern boundary of the North Atlantic Subtropical Gyre. *Journal of Geophysical Research: Oceans*, *115*(9). https://doi.org/10.1029/2010JC006161

G. Siedler, W. Zenk, & W. J. Emery. (1985). Strong Current Events Related to a Subtropical Front in the Northeast Atlantic. *Journal of Physical Oceanography*.

Galloway, T. S., Cole, M., & Lewis, C. (2017). Interactions of microplastic debris throughout the marine ecosystem. *Nature Ecology & Evolution 2017 1:5*, *1*(5), 1–8. https://doi.org/10.1038/s41559-017-0116

Greater Atlantic Regional Fisheries Office. (2020). *Lobster Management Areas*. https://www.fisheries.noaa.gov/resource/map/lobster-management-areas

Hernández-Guerra, A., Fraile-Nuez, E., López-Laatzen, F., Martínez, A., Parrilla, G., & Vélez-Belchí, P. (2005). Canary Current and North Equatorial Current from an inverse box model. *Journal of Geophysical Research: Oceans*, *110*(12), 1–16. https://doi.org/10.1029/2005JC003032

Herrera, A., Asensio, M., Martínez, I., Santana, A., Packard, T., & Gómez, M. (2018). Microplastic and tar pollution on three Canary Islands beaches: An annual study. *Marine Pollution Bulletin*, *129*(2), 494–502. https://doi.org/10.1016/J.MARPOLBUL.2017.10.020

Herrera, A., Rivera, J. A., Moreno, T., Martínez, I., & Gómez, M. (2022). First inventory of marine debris on Alegranza, an uninhabited island in the Northeast Atlantic. *Marine Pollution Bulletin*, *178*. https://doi.org/10.1016/J.MARPOLBUL.2022.113604

Hurlburt, H. E., & Hogan, P. J. (2000). Impact of 1/8°to 1/64°resolution on Gulf Stream model-data comparisons in basin-scale subtropical Atlantic Ocean models. *Dynamics of Atmospheres and Oceans*, *32*(3–4), 283–329. https://doi.org/10.1016/S0377-0265(00)00050-6

Jambeck, J. R., Geyer, R., Wilcox, C., Siegler, T. R., Perryman, M., Andrady, A., Narayan, R., & Law, K. L. (2015). Plastic waste inputs from land into the ocean. *Science*, *347*(6223), 768–771. https://doi.org/10.1126/SCIENCE.1260352

Josep L. PELEGRÍ, & Jesús PEÑA-IZQUIERDO. (2015). *Oceanographic and biological features in the Canary Current Large Marine Ecosystem*. http://hdl.handle.net/1834/9135

Krauss, W. (1986). The North Atlantic Current. *Journal of Geophysical Research*, *91*(C4), 5061. https://doi.org/10.1029/JC091IC04P05061

Lazier J. R. N., & Wright D. G. (1993). Annual Velocity Variations in the Labrador Current. *Journal of Physical Oceanography*, *23*, 659–678. https://doi.org/https://doi.org/10.1175/1520-0485(1993)023<0659:AVVITL>2.0.CO;2

Lynch, D. R., Ip, J. T. C., Naimie, C. E., & Werner, F. E. (1996). Comprehensive coastal circulation model with application to the Gulf of Maine. *Continental Shelf Research*, *16*(7), 875–906. https://doi.org/10.1016/0278-4343(95)00028-3

Machín, F., Hernández-Guerra, A., & Pelegrí, J. L. (2006). Mass fluxes in the Canary Basin. *Progress in Oceanography*, *70*(2–4), 416–447. https://doi.org/10.1016/j.pocean.2006.03.019

Mason, E., Colas, F., Molemaker, J., Shchepetkin, A. F., Troupin, C., McWilliams, J. C., & Sangrà, P. (2011). Seasonal variability of the Canary Current: A numerical study. *Journal of Geophysical Research: Oceans*, *116*(6). https://doi.org/10.1029/2010JC006665

Michael D. Cox, & Kirk Bryan. (1984). A Numerical Model of the Ventilated Thermocline. *Journal of Physical Oceanography*. https://doi.org/https://doi.org/10.1175/1520-0485(1984)014<0674:ANMOTV>2.0.CO;2

Miller, M. E., Hamann, M., & Kroon, F. J. (2020). Bioaccumulation and biomagnification of microplastics in marine organisms: A review and meta-analysis of current data. *PLOS ONE*, *15*(10). https://doi.org/10.1371/JOURNAL.PONE.0240792

NOAA - Climate Prediction Center. (2022). *North Atlantic Oscillation*. https://www.cpc.ncep.noaa.gov/products/precip/CWlink/pna/nao.shtml

Reinold, S., Herrera, A., Hernández-González, C., & Gómez, M. (2020). Plastic pollution on eight beaches of Tenerife (Canary Islands, Spain): An annual study. *Marine Pollution Bulletin*, *151*. https://doi.org/10.1016/J.MARPOLBUL.2019.110847

Sala, I., Harrison, C. S., & Caldeira, R. M. A. (2016). The role of the Azores Archipelago in capturing and retaining incoming particles. *Journal of Marine Systems*, *154*, 146–156. https://doi.org/10.1016/j.jmarsys.2015.10.001

Scientific Advice Mechanism's (SAM) Goup of Chief Scientific Advisors. (2019). Environmental and health risks of microplastic pollution. In *Publication Office of the European Union*. https://doi.org/https://data.europa.eu/doi/10.2777/65378

Sicre, M. A., Weckström, K., Seidenkrantz, M. S., Kuijpers, A., Benetti, M., Masse, G., Ezat, U., Schmidt, S., Bouloubassi, I., Olsen, J., Khodri, M., & Mignot, J. (2014). Labrador current variability over the last 2000 years. *Earth and Planetary Science Letters*, *400*, 26–32. https://doi.org/10.1016/J.EPSL.2014.05.016

State of Maine - Department of Marine Resources. (2018). *Numbers of Lobster Fishing Licenses and Trap Tags*. Science & Research. https://www.maine.gov/dmr/science-research/species/lobster/licenses-tags.html

State of Maine - Department of Marine Resources. (2022). *LOBSTER AND CRAB REGULATIONS*. https://www.maine.gov/dmr/laws-regulations/regulations/documents/Chapter25_05012022.pdf

Stramma, L. (1984a). Geostrophic transport in the Warm Water Sphere of the eastern subtropical North Atlantic. *Journal of Marine Research*, *42*, 537–558. https://doi.org/https://doi.org/10.1357/002224084788506022

Stramma, L. (1984b). Geostrophic transport in the Warm Water Sphere of the eastern subtropical North Atlantic. *Journal of Marine Research*, *42*, 537–558.

Stramma, L., & Müller, T. J. (1989). Some observations of the Azores Current and the North Equatorial Current. *Journal of Geophysical Research: Oceans*, *94*(C3), 3181–3186. https://doi.org/10.1029/JC094IC03P03181

Stramma, L., & Siedler, G. (1988). Seasonal Changes in the North Atlantic Subtropical Gyre. *JOURNAL OF GEOPHYSICAL RESEARCH*, *93*(C7), 8111–8118. https://doi.org/10.1029/JC093iC07p08111

Taylor, A. H., & Stephens, J. A. (1998). The North Atlantic Oscillation and the latitude of the Gulf Stream. *T Ellus*, *50*(1), 134–142. https://doi.org/10.3402/tellusa.v50i1.14517

Tychensky, A., le Traon, P. Y., Hernandez, F., & Jotirdan, D. (1998). Large structures and temporal change in the Azores Front during the SEMAPHORE experiment. *Journal of Geophysical Research: Oceans*, *103*(C11), 25009–25027. https://doi.org/10.1029/98JC00782

van Sebille, E., Aliani, S., Law, K. L., Maximenko, N., Alsina, J. M., Bagaev, A., Bergmann, M., Chapron, B., Chubarenko, I., Cózar, A., Delandmeter, P., Egger, M., Fox-Kemper, B., Garaba, S. P., Goddijn-Murphy, L., Hardesty, B. D., Hoffman, M. J., Isobe, A., Jongedijk, C. E., … Wichmann, D. (2020). The physical oceanography of the transport of floating marine debris. In *Environmental Research Letters* (Vol. 15, Issue 2). Institute of Physics Publishing. https://doi.org/10.1088/1748-9326/ab6d7d

van Sebille, E., Griffies, S. M., Abernathey, R., Adams, T. P., Berloff, P., Biastoch, A., Blanke, B., Chassignet, E. P., Cheng, Y., Cotter, C. J., Deleersnijder, E., Döös, K., Drake, H. F., Drijfhout, S., Gary, S. F., Heemink, A. W., Kjellsson, J., Monika Koszalka, I., Lange, M., … Zika, J. D. (2018). Lagrangian ocean analysis: Fundamentals and practices. *Ocean Modelling*, *121*, 1463–5003. https://doi.org/10.1016/j.ocemod.2017.11.008

Wang, S., Kenchington, E., Wang, Z., & Davies, A. J. (2021). Life in the Fast Lane: Modeling the Fate of Glass Sponge Larvae in the Gulf Stream. *Frontiers in Marine Science*, *8*. https://doi.org/10.3389/fmars.2021.701218

Watelet, S., Beckers, J. M., & Barth, A. (2017). Reconstruction of the Gulf Stream from 1940 to the Present and Correlation with the North Atlantic Oscillation. *Journal of Physical Oceanography*, *47*(11), 2741–2754. https://doi.org/10.1175/JPO-D-17-0064.1

Werner, F. E., Cowen, R. K., & Paris, C. B. (2007). Coupled Biological and Physical Models: Present Capabilities and Necessary Developments for Future Studies of Population Connectivity. *Source: Oceanography*, *20*(3), 54–69. https://doi.org/10.2307/24860096

Worthington, L. v. (1976). *On the North Atlantic circulation*. Johns Hopkins University Press.